JOURNAL OF MATERIALS SCIENCE 25 (1990) 2539–2548

Densification of silicon nitride ceramics under sinter–HIP conditions

I. ITURRIZA, J. ECHEBERRÍA, I. GUTIERREZ, F. CASTRO
Centro de Estudios e Investigaciones Técnicas de Guipúzcoa (CEIT), Apartado 1555, 20009 San Sebastian, Spain

The influence of several sinter–HIP variables on the densification behaviour of silicon nitride-based ceramics has been investigated. The processing conditions were studied for Si_3N_4 powder mixtures containing controlled amounts of Y_2O_3 + Al_2O_3 or Y_2O_3 + MgO. The specimens were subjected to sinter–HIP cycles under argon or nitrogen atmospheres at various temperatures and pressures. The final density of the powder compacts exhibited a strong dependence not only on the applied pressure, the composition and the processing temperature, but also on the pressurization rate and the initial pressurization time. The microstructural changes induced by the application of high pressure were followed by transmission electron microscopy. On examination by TEM, large concentrations of dislocations, generated inside some β-Si_3N_4 grains, were observed. Characterization of these dislocations showed that $\boldsymbol{b} = \langle 0\,0\,0\,1 \rangle$ is their most frequently found Burgers vector. Also, two relaxation mechanisms, tending to release the stored energy of deformation in the β-Si_3N_4 grains, namely grain penetration (a form of strain-induced boundary migration) and grain fragmentation (the formation of subgrains due to rearrangement of dislocations into low energy configurations), have been identified. The intergranular phases formed were characterized by energy dispersive X-ray spectroscopic analysis, X-ray diffraction and electron diffraction. The influence of different sinter–HIP cycles on the $\alpha \rightarrow \beta$ transformation of silicon nitride without additives was also investigated by X-ray diffractometry.

1. Introduction

The production of ceramics based on silicon nitride is of considerable interest because of their unique combination of chemical, physical and mechanical properties, which makes them an important class of materials for a wide range of applications at elevated temperatures. The most commonly used processing methods for consolidating silicon nitride powders into highly dense components are sintering and hot pressing. However, problems exist in attaining full density during processing of solids with a high degree of covalent bonding due to low diffusivities at temperatures below that at which thermal decomposition is dominant [1, 2].

The addition of sintering aids, able to form a liquid phase at the sintering temperature, is now well established as a viable route to achieve highly dense silicon nitride-based materials [3–7]; although the formation of secondary grain-boundary phases on solidification has the effect of reducing their high-temperature strength [8].

Hot isostatic pressing of encapsulated green compacts is an alternative processing route which offers the potential of hot-pressed material properties often combined with the ability to produce components having a complex shape [6, 9–12]. A particular advantage of this processing method is that the gas pressure is uniformly applied in all directions and is typically higher than that used during uniaxial hot pressing. Under these conditions, high densities can be achieved, both at lower temperatures than those used during pressureless sintering thus preventing thermal decomposition and grain growth or by adding lesser amounts of sintering aids thus decreasing the volume fraction of secondary phases formed upon cooling.

Sinter–HIP is another route, which involves processing of non-encapsulated green compacts while the benefits of the application of high pressure during consolidation can still be obtained. In this method the green compacts are sintered and subsequently hot-isostatically pressed during the same cycle [13, 14]. In the present work, the green compacts were subjected to sinter–HIP cycles in argon or nitrogen atmospheres, the initial sintering stage being performed under a gas pressure of 0.5 MPa in order to avoid thermal decomposition of the specimens.

The purpose of this research work was to investigate the influence of the sinter–HIP processing parameters on the densification behaviour of silicon nitride with varying amounts of oxide additions. The resulting microstructures were examined by transmission electron microscopy. The glassy or crystalline character of the resulting intergranular phases and the relative changes in composition between them were studied by electron diffraction and energy dispersive X-ray spectroscopy (EDS), respectively.

0022–2461/90 $03.00 + .12

Additionally, the $\alpha \rightarrow \beta$ transformation was investigated by X-ray diffraction (XRD) in terms of the processing variables.

2. Experimental procedure

The experimental powder used was commercial silicon nitride (91% α-Si_3N_4) with a specific surface area of $12\,m^2\,g^{-1}$ (BET) and the following chemical composition in wt%: 0.4Si (free), 0.08Fe, 0.04Al, 0.01Ca, 0.048C, 1.5 oxygen, Si_3N_4 (balance). Mixtures were obtained by adding controlled amounts of Al_2O_3 (>99% pure) or MgO (>99.5% pure) to the basic silicon nitride plus yttria (99.9% pure) powder. The mixtures were based on the addition of varying amounts of alumina or magnesia, never exceeding the concentration of Y_2O_3 in wt %, to the basic combinations of Si_3N_4 + 3 wt % Y_2O_3 and Si_3N_4 + 6 wt % Y_2O_3. The desired mixtures were prepared by dry milling the blended powders for 48 h using a ball mill consisting of a polyethylene container and silicon nitride milling media. Green compacts were produced by uniaxial pressing of 2.5 g powder samples taken from these mixtures. Powder compaction was carried out using a 16 mm internal diameter rigid steel die, and applying a compaction pressure of 100 MPa, which results in compacts having densities between 52 and 57% theoretical on composition.

Before sintering, the compacts were placed in a graphite crucible coated with boron nitride in order to protect them from contamination. The specimens were located inside the coated crucible using a powder bed containing equal proportions of Si_3N_4 and BN. Sintering was performed at a temperature of 1750° C in a graphite-heated furnace under argon or nitrogen atmospheres at a pressure of 0.5 MPa. This pressure was maintained constant during the whole heating period (from room temperature to the sintering temperature at a rate of $30°\,C\,min^{-1}$) and subsequently increased according to the different sinter–HIP schedules. A schematic illustration of the type of sinter–HIP cycles used is presented in Fig. 1. The experiments were performed using an ASEA–HIP (QIH-6) equipment, gas pressures between 10 and 150 MPa during the HIPing part of the cycles and temperatures between 1750 and 1850° C. A constant time $t_s = t_f - t_h = 60$ min (see Fig. 1) was invariably employed in every cycle and defined as the sintering time, that is, from the moment the specimens reached the sintering temperature (t_h) to the start of the cooling period.

In the figure, t_i represents the time elapsed between t_h and the moment at which the gas pressure was increased. For convenience, a cycle in which t_i is, for instance, 30 min and the target pressure is reached in 10 min will be called a 30–10–20 cycle, where 20 represents the holding time at pressure (t_m) at the processing temperature (T_s). Other cycles will also be referred to in a similar way.

The characterization of the α–β transformation was carried out, on polished samples, by X-ray diffractometry using monochromic Cu$K\alpha$ radiation. The $\alpha:\beta$ silicon nitride ratios were calculated using a standard procedure [15] based on measurements of the ratio of intensities of the $\alpha_{21.0}$ and $\beta_{21.0}$ reflections.

For microstructural analysis in the electron microscope, discs were obtained from bulk specimens using a diamond cutting wheel to obtain sections ~0.5 mm thick and followed by a coring operation using a 3 mm internal diameter diamond coring tool. The discs were mechanically ground to a thickness of about 0.2 mm, dimpled to ~20 μm and ion milled to electron transparancy. A thin film of carbon was evaporated on to the foil to avoid charging during exposure to the electron beam. Analysis of thin foils was subsequently carried out using a Philips CM-12 scanning transmission electron microscope fitted with an EDAX system and a LaB_6 filament. An accelerating voltage of 100 kV was invariably selected.

3. Results and discussion

The simultaneous application of pressure and temperature during sintering of silicon nitride-based ceramics, tending to produce fully dense components, is a process which requires detailed knowledge of the influence that different sinter–HIP schedules exert on their densification behaviour. The results presented in this work show that variables such as the starting pressurization time (t_i), the holding time at pressure (t_m) and the pressurization rate (P_r) must be taken into consideration, along with pressure (P) and the sintering temperature (T_s) during densification of silicon nitride-based ceramics by a containerless sinter–HIP

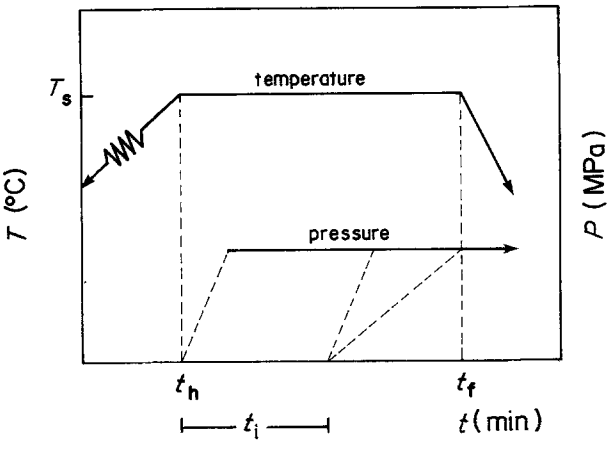

Figure 1 Schematic representation of the experimental sinter–HIP cycles. The sinter–HIP time defined as $t_f - t_h = 60$ min was kept constant.

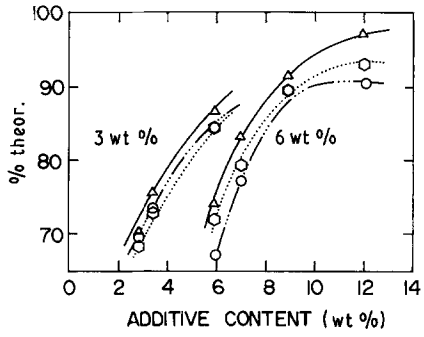

Figure 2 Theoretical density–additive content relationship showing the influence of t_i for specimens processed at 1750° C in an argon atmosphere. The indicated 3 and 6 wt % represent wt % Y_2O_3 in the powder mixture, and this convetion is used for all the figures. (△) 10 MPa, 30–10–20, (○) 10 MPa, 0–10–50, (○) 0.5 MPa.

TABLE I Final densities (% theor.) obtained for several compositions (Si_3N_4 + Y_2O_3 + Al_2O_3) after different sinter–HIP cycles at 10 MPa argon pressure and 1750° C

Additive content (wt %) Y_2O_3 + Al_2O_3		Density (% theoretical)			
		Sinter–HIP cycles			Pressureless 60–0–0*
		0–10–50	15–10–35	30–10–20	
3	0	70.1	70.6	70.3	68.7
3	0.5	74.3	73.9	75.7	73.2
3	3	84.8	84.3	86.5	84.6
6	0	67.1	72.3	74.2	72.4
6	1	77.6	79.4	83.3	79.3
6	3	89.2	88.9	91.2	89.4
6	6	90.2	96.8	96.6	92.6

*The "pressureless" cycle was carried out at 0.5 MPa constant argon pressure at 1750° C for 60 min.

route. This is illustrated for several ceramic alloys of differing chemical composition within the Si_3N_4–Y_2O_3–Al_2O_3 or the Si_3N_4–Y_2O_3–MgO systems in Figs 2 to 4.

Fig. 2 shows, for a group of specimens containing additions of Y_2O_3 and Al_2O_3, that t_i determines to a large extent the final density achieved. This is illustrated in the figure, and in Table I, by comparing different sinter–HIP cycles performed at 10 MPa. These results are also compared to those obtained after sintering under a constant argon pressure of 0.5 MPa. It is noteworthy that applying high pressure (10 MPa in these cases) during the sinter–HIP cycle does not necessarily yield higher specimen densities. An increasing argon pressure applied at the beginning of the cycle (t_i = 0) leads, in fact, in most cases, to a decrease in the ultimate density achieved as compared to that obtained after low-pressure (0.5 MPa) sintering. In contrast, increasing the pressure, after allowing 30 min (i.e. t_i = 30 min) sintering at low pressure, results, for all compositions, in specimens of higher final density.

It must be emphasized that these sinter–HIP cycles were performed keeping a constant pressurization rate, P_r, of 1.0 MPa min^{-1} and a maximum pressure of 10 MPa. The influence of t_i on the final density, could therefore be understood by considering the amount and type of porosity contained in each specimen at the moment the pressure was increased. Thus, for any fixed composition (see Fig. 2 and Table I), the application of high pressure after long sintering periods (increasing t_i), results in specimens of higher density, because of their lower content of open porosity with respect to specimens subjected to cycles with a shorter (t_i small) pressureless sintering time. This is an obvious consequence of the fact that the benefits of HIPing on densification can only be obtained through closure of porosity not connected to the surface of the specimen. In contrast, the almost negligible, or actually negative (compare results of low-pressure sintering to those of cycle 0–10–50 in Fig. 2) influence of pressure on the final density of specimens subjected to cycles with a "too early" application of pressure (t_i small), is related to argon entrapment within the pores and the development of an internal hydrostatic pressure which acts as an opposition to the elimination of porosity. It can therefore be concluded that using larger t_i values favours the attainment of higher final densities, because "gas leaking" into the porosity of the ceramic specimens is reduced (or totally prevented) due to closure of larger amounts of open and interconnected porosity during the low-pressure part of the cycle. The same trend can also be observed by considering the results as a function of composition. As shown in Fig. 2, the application of high pressure has a more marked effect on density for specimens containing larger amounts of sintering aids (i.e. which sinter in the presence of larger amounts of liquid). In this case, this is due to their more advanced densification stage at the moment the pressure is applied, although there may also be an additional contribution due to the fact that larger amounts of liquid could assist the transmission of pressure in a more efficient manner.

The influence of pressurization rate on density can be noticed by referring to Figs 3a and b, for a set of specimens subjected to sinter–HIP cycles, during which both the maximum gas pressure, P = 10 MPa,

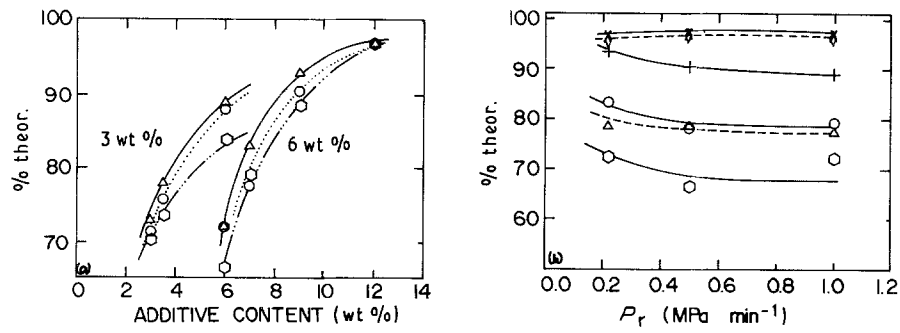

Figure 3 (a) Theoretical density–additive content relationship for specimens processed in argon at 1750° C under 10 MPa and different pressurization rates, (P_r), (△) 15–45–0, (○) 15–20–25, (○) 15–10–35; and (b) theoretical density as a function of P_r. A, M and Y represent alumina, magnesia and yttria respectively. (◇) 6Y6M, (×) 6Y6A, (+) 6Y3A, (△) 6Y1M, (○) 6Y1A, (○) 6Y. The numbers indicate the amounts added in wt %.

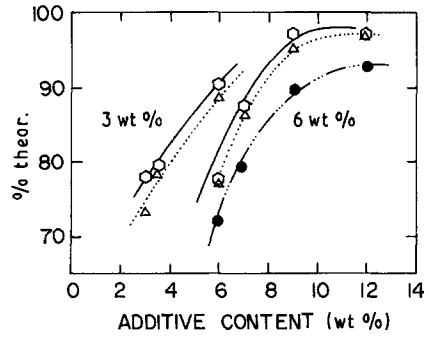

Figure 4 Theoretical density as a function of additive content for specimens processed at various ultimate pressures, at 1750° C in argon and keeping constant values of P_r = 3.3 MPa min^{-1} and t_i = 30 min. (●) 0.5 MPa, (△) 50 MPa, 30–15–15, (○) 100 MPa, 30–30–0.

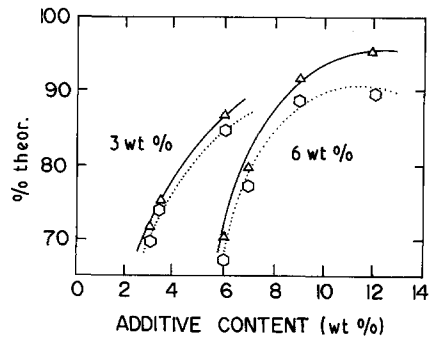

Figure 5 Relationship between theoretical density and additive content for specimens processed at 1750° C and 10 MPa pressure during a 0–10–50 sinter–HIP cycle. (△) Nitrogeon atmosphere, (○) argon atmosphere.

and the starting pressurization time, t_i = 15 min, have been kept constant. As observed in Fig. 3b, and for a given composition, the general trend indicates an increase in the final density as the pressurization rate (P_r) decreases. This behaviour also seems to be related to the densification stage associated with the specimens at the moment the pressure is increased, because a high pressurization rate implies reaching the working pressure in a short time, therefore increasing the possibility of "gas-leaking" into the pores. On the other hand, using a "low" pressurization rate permits attaining higher densities of the specimens before "full" pressure is applied, thus diminishing the possibilities for gas entrapment and producing higher final densities. Fig. 3b also shows that the effect of P_r on density becomes negligible, as may be expected, for compositions (large amounts of sintering aids in this case) which exhibit a high densification rate during the pressureless sintering part of the cycle. In addition, it is also apparent from the figure that, substituting alumina by magnesia produces a very similar effect, although it must be emphasized that specimens containing magnesia showed weight losses of up to 1%.

Fig. 4 shows that sinter–HIP, with large initial pressurization times (t_i) and high argon pressures, produce higher densities in specimens of all compositions, compared to the data points obtained by low-pressure sintering. These results substantiate the reduction of weight losses and the enhanced densification rate produced by the application of high pressure. As observed in the figure, the increase in density is approximately constant for all compositions, although there is a slightly larger effect on specimens containing higher amounts of Al_2O_3. This behaviour could be attributed to two different reasons. First, the application of pressure enhances the rearrangement process which is, in turn, more effective in the presence of sufficiently large quantities of liquid; and second, the larger capillary pressure developed, and enhancement of dissolution, lead to higher densities as diffusion through a low-viscosity liquid (higher Al_2O_3 contents) takes place. On the other hand, the only marginal increase in density obtained by increasing the pressure from 50 to 100 MPa, suggests that for systems which form a liquid phase at the sintering temperature, the optimum pressure that has to be applied is not necessarily the highest available. In addition, as reported in Table II, the behaviour observed using MgO instead of Al_2O_3 is similar to that described above. However, the lower densities achieved using MgO as a secondary additive reflect, as shown in the table by the weight losses, its tendency to volatilize during sintering.

The influence of a nitrogen atmosphere is shown in Fig. 5. As observed in the figure, the densification process follows approximately the same trend as with argon. Using nitrogen, however, increases the densification kinetics producing a nearly constant increase in density of about 3% to 4% for all alumina concentrations. This increase is not surprising because nitrogen is a reactive gas in this ceramic system, which prevents entrapment of a non-reactive gas in the pores. It is also noticeable, by comparing this figure with Fig. 2, that using nitrogen in a cycle with t_i = 0 (Fig. 5) results in very similar final densities to those obtained with argon in a cycle with t_i = 30 min

TABLE II Theoretical density and weight change of Si_3N_4-based specimens after sinter-HIP cycles carried out at 1750° C with t_i = 30 min and P_r = 3.3 MPa min^{-1}

Additive content (wt %)				Sinter–HIP cycles			
Y_2O_3 + Al_2O_3		Y_2O_3 + MgO		30–15–15 (50 MPa)		30–30–0 (100 MPa)	
				% theor.	Δ wt %	% theor.	Δ wt %
6	0			77.1	−1.7	77.5	−1.3
6	1			86.3	−0.7	87.4	−0.5
6	3			95.3	−0.3	97.2	−0.1
6	6			96.8	−0.1	97.1	−0.3
		6	1	79.6	−2.9	80.1	−2.6
		6	3	92.3	−1.9	94.8	−1.5
		6	6	91.6	−2.0	94.0	−1.9

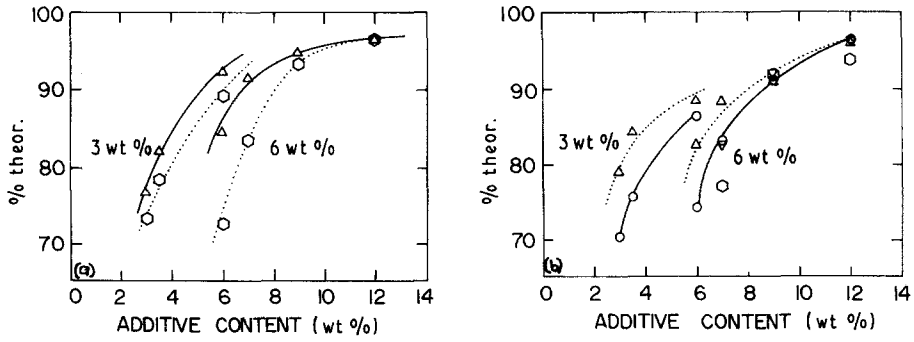

Figure 6 Theoretical density–additive content relationship for specimens processed in argon at 10 MPa after (a) isothermal 15–45–0 sinter–HIP cycles at (○) 1750° C and (△) 1825° C and (b) non-isothermal 30–10–20 sinter–HIP cycle at (○, ○) 1750° C, and (△, ▽) with a rise in temperature to 1850° C for 10 min after 30 min at 1750° C. (▽, ⬡) Specimens containing MgO instead of Al_2O_3.

(Fig. 2). Applying higher nitrogen pressures would therefore be expected to produce densities even closer to theoretical than those shown in the figure.

The influence of temperature, is illustrated in Figs 6a and b. Fig. 6a shows, for identical sinter–HIP cycles (15–45–0, 10 MPa in argon), the effect of a higher thermal activation on the densification process. It is noteworthy, that for specimens containing 3 wt % Y_2O_3 mixed with up to 3 wt % Al_2O_3 an increase in temperature produces an almost constant increase in density at all compositions; however, for specimens containing 6 wt % Y_2O_3 mixed with up to 6 wt % Al_2O_3, a stronger effect is observed for lower Al_2O_3 contents. As observed in Fig. 6b, a similar response was obtained after a non-isothermal heating, from 1750 to 1850° C, during the sinter–HIP cycle (30–10–20 in this case). This response could be understood by considering the viscosity of the liquid phase formed, together with the type and amount of residual porosity in the specimens. Therefore, for specimens containing "larger" amounts of porosity (e.g. low in Al_2O_3), which may in large proportion be located at grain boundaries, a reduction in the viscosity of the liquid, caused by an increase in temperature, could produce a substantial acceleration of the densification kinetics by facilitating the diffusion of material; whereas, for denser specimens the elimination of residual porosity may be limited to a certain extent by the occurrence of grain growth activated by exposing the ceramic to higher temperatures.

Also, as illustrated in the same figure, the use of MgO as a substitution for Al_2O_3, results in a similar response; however, a larger dispersion of the data points and lower final densities are observed in general. This latter point can be clearly appreciated in the figure by noticing that the densities attained by sintering MgO-containing specimens at the higher temperature (1750 + 1850° C) are the same as those obtained after sintering of Al_2O_3-containing samples at the lower temperature of 1750° C.

The $\alpha \rightarrow \beta$ phase transformation is a characteristic transition during sintering of α-Si_3N_4 powder compacts. Fig. 7 shows the influence of several sinter–HIP schedules on the amount of β-Si_3N_4 present in specimens of "pure" silicon nitride after processing. Some remarks are worth mentioning: (a) "pure" silicon nitride had to be used for this analysis because using additives generally leads to a fast and complete transformation under those processing conditions, (b) larger additions of sintering aids (e.g. Y_2O_3 or Y_2O_3 + Al_2O_3) result in the formation of larger amounts of liquid thus producing a substantial increase in the transformation kinetics with respect to the behaviour of "pure" Si_3N_4, (c) the comparison between the transformation and densification kinetics leads to the conclusion, in general, that for "pure" silicon nitride as well as for the Si_3N_4–Y_2O_3 and Si_3N_4–Y_2O_3–Al_2O_3 systems the transformation is by far faster than densification, and (d) the transformation is a thermally activated process which takes place progressively in time.

Based on these remarks, on previously reported data [5, 16] and on the results presented in Fig. 7, it can be realized that for (Si_3N_4, Si_3N_4 + Y_2O_3 or Si_3N_4 + Y_2O_3 + Al_2O_3) the processing parameters which aid densification also encourage the transformation. However, these phenomena occur at completely different rates, so that in contrast with the results reported by some authors [17] substantial densification may take place after the phase transformation has been completed. From the figure, it is also apparent that increasing the pressure in one order of magnitude results in an increase of about 2 to 3 times, of the β-phase present in the specimen. However, an increase of 100° C in temperature causes a change, of about 5 times, in the amount of β, so producing a fully transformed specimen. This marked effect of temperature on the $\alpha \rightarrow \beta$ transformation, may be due to lower viscosity of the liquid, which allows a steep composition gradient to be maintained around the α particles;

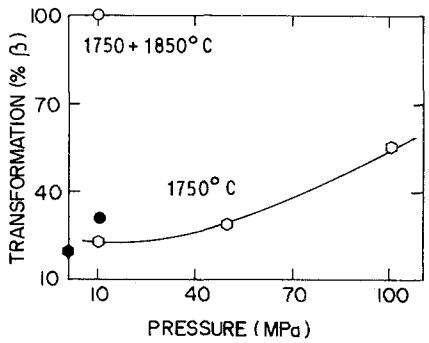

Figure 7 Dependence of %β on pressure and temperature, for specimens of pure silicon nitride processed in an argon atmosphere. The indicated temperatures correspond to the sintering temperature. (○) 30–10–20, (○) 30–30–0. (⬡) 0.5 MPa constant pressure at 1750° C; (●) 30–10–20 cycle at 1750° C.

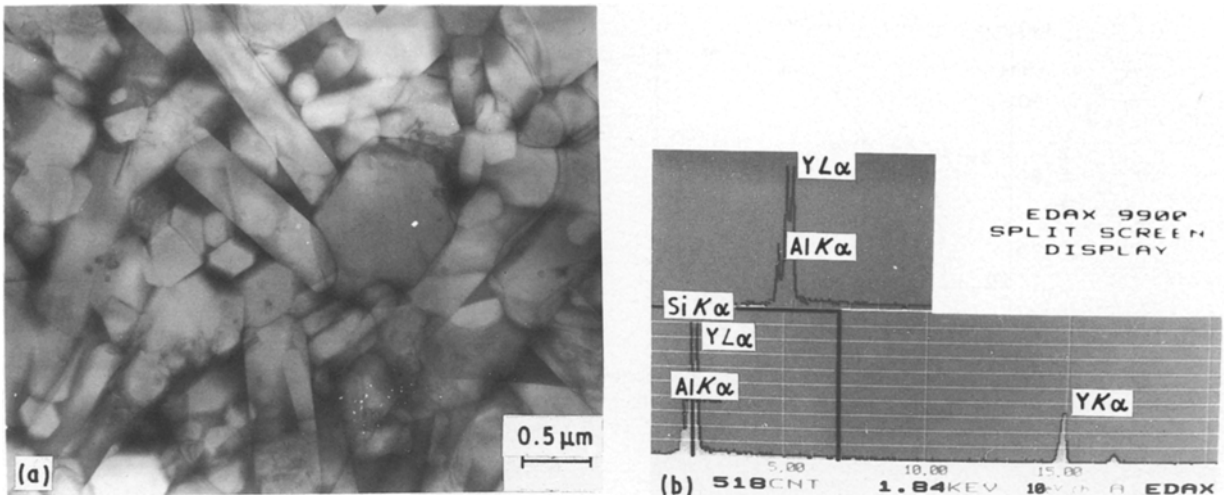

Figure 8 (a) Transmission electron micrograph corresponding to a dense Si_3N_4 + 6% Y_2O_3 + 6% Al_2O_3 specimen. (b) EDS analysis of the intergranular glassy phase (dark area in the micrograph).

therefore, allowing larger quantities of α-Si_3N_4 to be dissolved and subsequently precipitated as β-Si_3N_4.

From the observation of specimens, carried out by TEM, it was found that under the experimental conditions, sinter–HIP of Si_3N_4 with additions of Y_2O_3 and Al_2O_3 proceeds with the formation of a microstructure which contains elongated β-grains, porosity, crystalline and glassy yttria-rich intergranular phases, in varying proportions depending on composition and processing conditions.

The micrograph in Fig. 8a, which corresponds to a fully transformed specimen containing Si_3N_4 + 6% Y_2O_3 + 6% Al_2O_3, shows the presence of an yttrium-rich intergranular glassy phase (dark) surrounding the β-Si_3N_4 grains. A qualitative EDS analysis obtained from this intergranular phase is shown in Fig. 8b. It reveals the presence of silicon and aluminium as additional constituents of its composition in agreement with previously reported data [18]. In contrast to the microstructure observed for specimens containing a low ratio of Y_2O_3/Al_2O_3 (in wt %) as part of their chemical composition, crystalline second phases were observed for specimens containing none or only small amounts of alumina. Fig. 9a shows an area of a specimen of initial composition Si_3N_4 + 20% Y_2O_3 + 2% Al_2O_3 which exhibits hexagonal β-grains surrounded by a crystalline (see Fig. 9b) second phase whose composition (Fig. 9c) is higher in yttrium and lower in aluminium than that in Fig. 8b.

The application of pressure during processing of the specimens did not seem to have an effect on the crystalline character of the intergranular phase and only depends apparently, on the Y_2O_3/Al_2O_3 ratio and the cooling conditions. It is interesting to observe, however, that independently of the distribution of

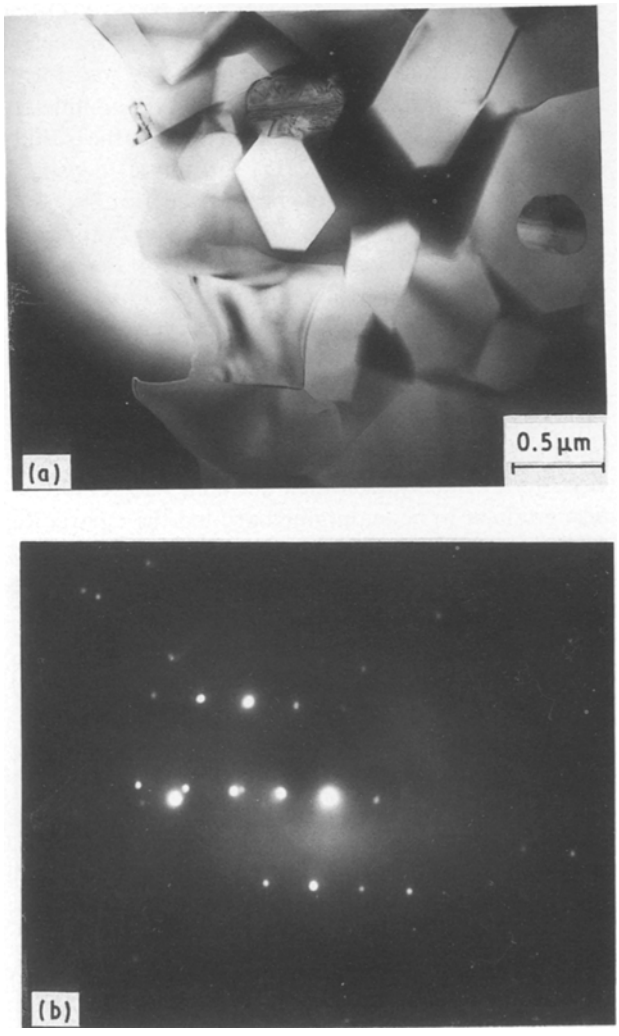

Figure 9 Transmission electron micrograph corresponding to a dense Si_3N_4 + 20% Y_2O_3 + 2% Al_2O_3 specimen, (b) electron diffraction pattern of the intergranular second phase, and (c) EDS analysis of the intergranular crystalline phase.

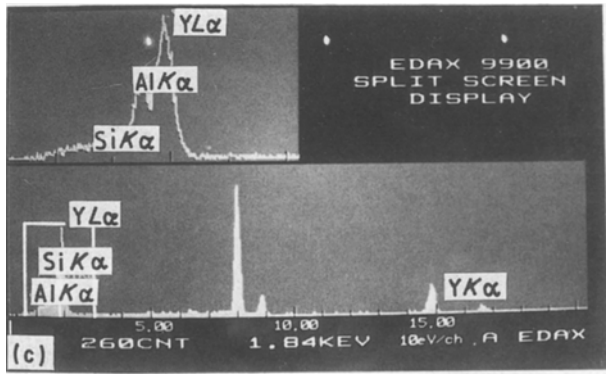

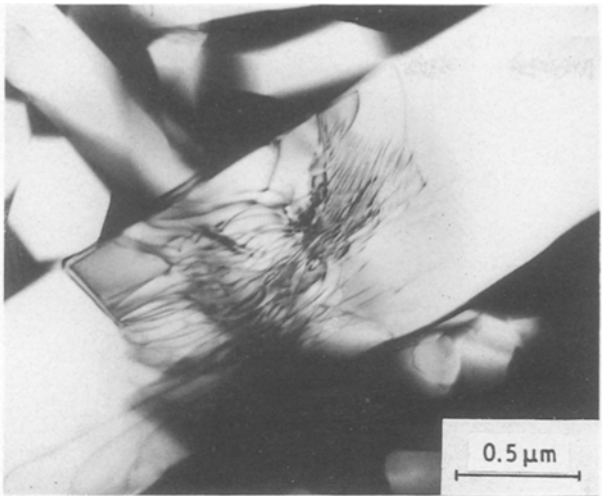

Figure 10 Transimission electron micrograph showing a β-Si_3N_4 elongated grain with dislocations in its interior which lie predominantly in a single direction.

these phases and their crystalline character, there always seems to be a thin layer of glass (>0.8 nm) surrounding the β-grains or separating the crystalline intergranular phase and the neighbouring β-grains. This observation is in agreement with data reported previously [14, 19].

Closer examination by TEM of the microstructures exhibited by the specimens subjected to sinter–HIP revealed the presence of large concentrations of dislocations, generated in some β-grains, due to the application of pressure during the sinter–HIP cycle. This observation provides direct evidence of plastic deformation; taking place, however, to a limited extent because the dislocations lie predominantly in a single direction (e.g. Figs 10 and 12a) and only in a relatively small fraction of larger β-Si_3N_4 grains. A systematic analysis of the Burgers vectors of these dislocations (e.g. those in the grain shown in Fig. 10 under a multi-beam condition), using a series of two-beam conditions, showed that most satisfy the invisibility criterion $\mathbf{g} \cdot \mathbf{b} = 0$ for reflections of the form $\{0\,1\,\bar{1}\,0\}$, $\{1\,1\,\bar{2}\,0\}$ and $\{1\,2\,\bar{3}\,0\}$ and therefore have a $\langle 0\,0\,0\,1\rangle$ Burgers vector (Fig. 11). These features are entirely consistent with the observations by Evans and Sharp [20] in a reaction-bonded Si_3N_4 subjected to compression at 1400° C, except that in the present case the generation of dislocations occurs during processing. Under these conditions, however, and because of the thermal energy supplied during the cycle, the microstructure is unstable and will, under favourable circumstances, tend to release the stored energy of deformation. Two different processes of relaxation have been observed during the present work and can be appreciated by reference to the micrographs in Fig. 12.

Fig. 12a shows the bulging of high-angle boundaries (arrowed in the micrograph) due to the difference in stored energy between the adjacent grains. The basis of this phenomenon, termed "grain penetration" and observed before in silicon nitride [14], is the annihilation of defects, generated during deformation, by the sweeping action of the boundary which acts as a sink for such defects (e.g. dislocations), and is similar to the process of strain-induced boundary migration (SIBM) first reported in metallic systems [21, 22]. The main distinction between these two processes is that strain-induced boundary migration takes place by the atomic jumps across the boundary, whereas in grain penetration there is always a thin layer of liquid in between the two grains. In the latter case, therefore, the movement of material may occur by different mechanisms which could actually involve diffusion through the liquid (e.g. solution–diffusion–precipitation). Nevertheless, the energetics of these two processes is based upon similar concepts, so that grain penetration, which involves the bulging of a high-angle boundary, will only take place if the substitution of distorted material by a dislocation-free crystal is energetically favourable. Using the theoretical criterion proposed by Bailey and Hirsch [23], for bulging to occur, in terms of the stored energy difference, $\Delta E'$, per unit volume across the migrating boundary and the grain-boundary surface energy, γ, the boundary will tend to bulge if the following relation is satisfied

$$\Delta E' > \frac{2\gamma}{L} \qquad (1)$$

where $2L$ is the length of boundary that bows out.

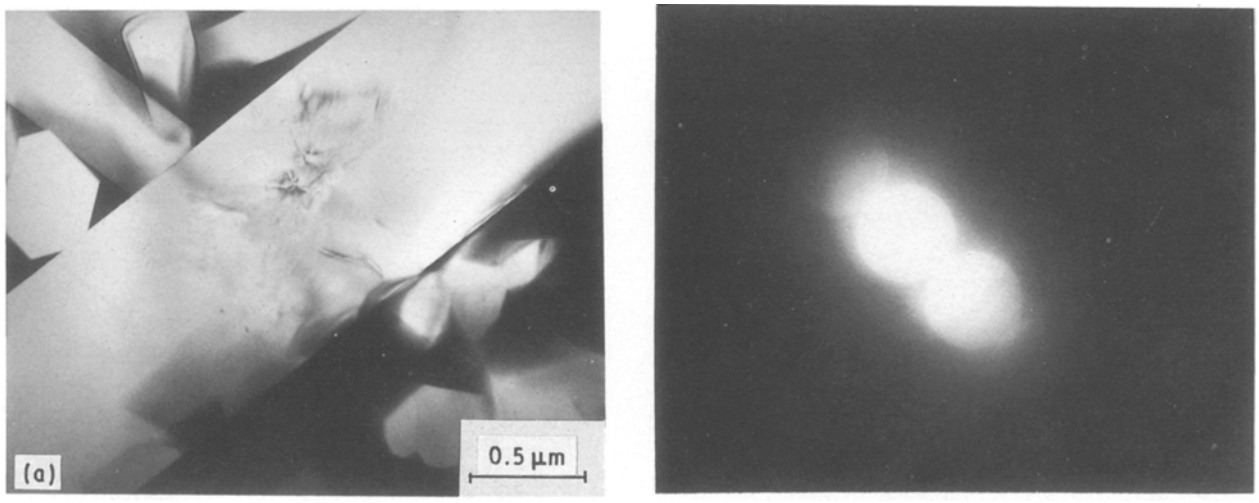

Figure 11 Two-beam convergent diffraction patterns and corresponding images for reflected beams with Miller indices (a) $\{0\,1\,\bar{1}\,0\}$, (b) $\{1\,1\,\bar{2}\,0\}$ and (c) $\{1\,2\,\bar{3}\,0\}$.

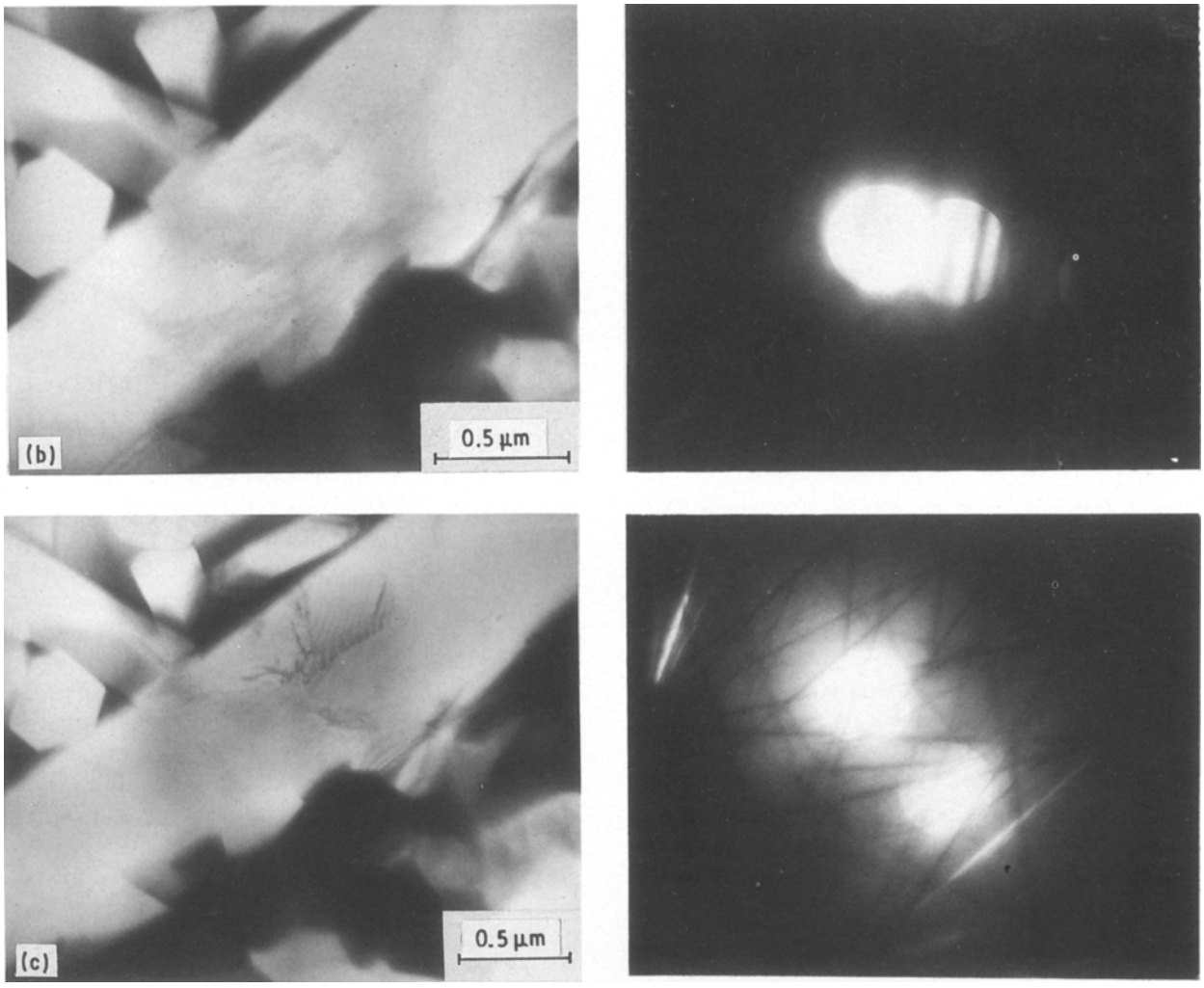

Figure 11 Continued.

This means, therefore, that for bulging to operate the dislocation density difference $\Delta\rho$ across the boundary must be sufficiently large, since $\Delta E'$ can be expressed as

$$\Delta E' = \alpha' G\boldsymbol{b}^2 (\Delta\varrho) = \alpha' \frac{E\boldsymbol{b}^2}{2(1+\nu)} (\Delta\varrho) \quad (2)$$

where $\alpha' = 0.5$ to 1.0, G is the shear modulus, ν the Poisson's ratio, E the Young's modulus and $\boldsymbol{b}$ the Burgers vector. Additionally, the surface energy $\gamma_{\alpha\beta}$ of an α/β interface can be written as [24]

$$\gamma_{\alpha\beta} < \frac{0.05}{6} E\boldsymbol{b} \quad (3)$$

Thus, combining these equations gives

$$\Delta\varrho > \frac{0.1}{3\alpha' \boldsymbol{b}L} (1+\nu) \quad (4)$$

and for the present material, typical values of the

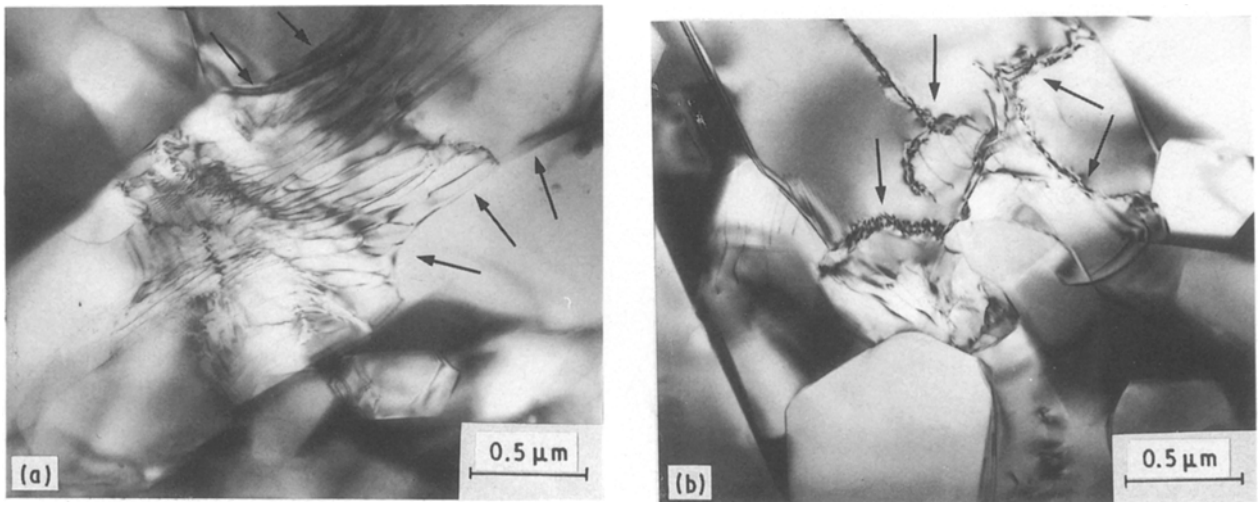

Figure 12 Transmission electron micrographs of specimens subjected to sinter-HIP, showing (a) "grain penetration", and (b) "grain fragmentation".

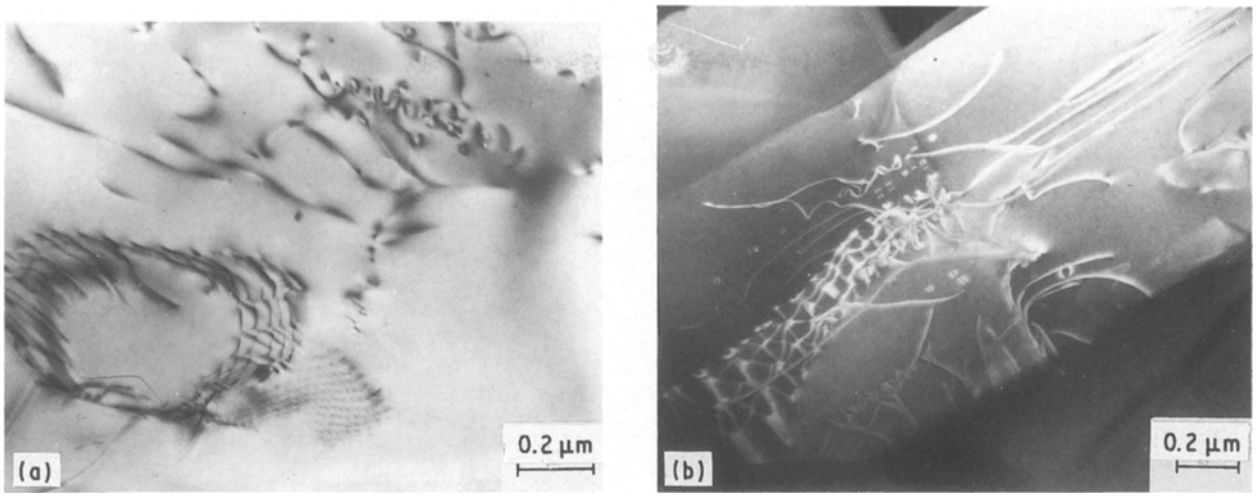

Figure 13 Transmisson electron micrographs of dislocation structures in β-Si_3N_4 exhibiting, (a) well-developed networks, and (b) dislocation wall with a complex structure.

parameters for calculation of the right-hand term in Equation 4 are: $\nu = 0.24$, $\boldsymbol{b} = 7 \times 10^{-10}$ m, $\alpha' = 0.5$ and L can be taken as one-half of the width of the elongated β-grains, that is, $\sim 0.3 \times 10^{-6}$ m. Substitution of these values in Equation 4 leads to

$$\Delta\varrho > 4 \times 10^{14}\ \mathrm{m}^{-2} \qquad (5)$$

which is a condition that, in spite of the approximate nature of the calculations, is in obvious agreement (see Figs 10 and 12a) with the experimental observations.

In addition, Fig. 12b shows a second relaxation process, termed "grain fragmentation", which is based upon rearrangement of dislocations in low-energy configurations. By this process the formation of subgrains, separated by low-angle boundaries (arrowed on the micrograph), involves changes in the dislocation arrays without the intervention of migration of high-angle boundaries. Thus, this is a process of recovery which requires thermal activation and results in the formation of dislocation walls (low-angle boundaries) due to the reduction of total elastic energy of the dislocations because of clustering. It is noteworthy, that during recovery, well-developed dislocation networks are often observed (e.g. Fig. 13a), although in some other instances, like that shown by a dark-field image in Fig. 13b, the subgrain boundaries develop a more complex structure. In both cases, however, the subboundary is constituted by dislocations with different Burgers vectors (not determined), and are also likely to be formed by mixed edge-screw dislocations.

4. Conclusions

Sinter–HIP, employed as a means for the production of fully dense silicon nitride components, is a very convenient processing route because the use of an encapsulant is not required; however, it demands close control of the processing schedule because of the strong dependence of the final density on the following variables: starting pressurization time (t_i), holding time at pressure (t_m), pressurization rate (P_r), ultimate pressure (P) and temperature (T_s).

The chemical composition of the powder mixture is obviously an important factor in any densification process, but much more so during sinter–HIP, because it is particularly important to choose the correct value of the parameters mentioned above in accordance with the amount of sintering aids added to the basic Si_3N_4 powder. In this context, especially when a non-reactive gas is used as the pressurizing medium, t_i is most critical, for maximum efficiency from the sinter–HIP cycle may only be gained when pressure is applied on components which are in a close porosity stage. On the other hand, variables such as pressurization rate or pressure exert little influence on systems which develop large quantities of liquid at the sintering temperature.

Sinter–HIP has an important influence on the microstructure of the ceramic specimens; not only because the $\alpha \rightarrow \beta$ transformation is encouraged by the application of high pressure, but also because it produces plastic deformation in a certain fraction of larger β-grains as evinced by the presence of large concentrations of dislocations within them. In many instances the $\langle 0\,0\,0\,1 \rangle$ is the most commonly found Burgers vector associated with these dislocations. As the dislocations are generated during processing of the ceramic specimens the microstructure is unstable, and because of the thermal energy supplied during the cycle, it will tend to release the stored energy of deformation. Two different relaxation mechanisms have been identified during this work: grain penetration and grain fragmentation. The former involves the bulging of grain boundaries in a similar way to strain-induced boundary migration, and the latter is based upon the rearrangement of dislocations in low-energy configurations.

Acknowledgements

The authors gratefully acknowledge the financial support received from Consejo Interministerial de Ciencia y Tecnología de España (CICYT) for the realization of this work.

References

1. G. ZEIGLER, J. HEINRICH and G. WÖTTING, *J. Mater. Sci.* **22** (1987) 3041.
2. P. POPPER, "Problems in sintering silicon nitride", in Proceedings of the International Symposium on "Factors in

densification and sintering of oxide and non-oxide ceramics", edited by S. Somiya and S. Saito (Tokyo, Japan, 1979) pp. 19–27.
3. G. R. TERWILLIGER and F. F. LANGE, *J. Amer. Ceram. Soc.* **57** (1974) 25.
4. S. HAMPSHIRE and K. H. JACK, "The kinetics of densification and phase transformation of nitrogen ceramics", in "Special Ceramics 7"; Proceedings of the British Ceramic Society, edited by D. Taylor and P. Popper (British Ceramics Society, Stoke on Trent, 1981) pp. 37–49.
5. L. J. BOWEN, T. G. CARRUTHERS and R. J. BROOK, *J. Amer. Ceram. Soc.* **61** (1978) 335.
6. G. WÖTTING and G. ZIEGLER, "Influence of powder properties and processing conditions on microstructure and properties of sintered Si_3N_4," in "Ceramic powders", edited by P. Vincensini (Elsevier, Amsterdam, 1983) pp. 951–62.
7. F. F. LANGE, *Int. Met. Rev.* **247** (1980) 1.
8. J. T. SMITH and C. L. QUACKENBUSH, "A Study of sintered Si_3N_4 compositions", in Proceedings of the International Symposium on "Factors in densification and sintering of oxide and non-oxide ceramics", edited by S. Somiya and S. Saito (Tokyo, Japan, 1979) pp. 426–42.
9. H. T. LARKER, "Dense ceramic parts hot pressed by hip", in "Emergent process methods for high-technology ceramics", Vol. 17, edited by R. F. Davies, H. Palmour and R. L. Porter (Plenum, New York, 1984) pp. 571–82.
10. *Idem,* "On hot isostatic pressing of shaped ceramic parts" in Proceedings of the Conference on "Ceramics in Engines", edited by S. Somiya, E. Kanai and K. I. Ando (Scientific Publications, Tokyo, Japan, 1984) Hakone, Japan, October 1983.
11. O. YEHESKEL, Y. GEFEN and M. TALIANKER, *J. Mater. Sci.* **19** (1984) 745.
12. *Idem, Mater. Sci. Engng.* **78** (1986) 209.
13. C. GRESKOVICH, *J. Amer. Ceram. Soc.* **64** (1981) 725.
14. I. ITURRIZA, F. CASTRO and M. FUENTES, *J. Mater. Sci.* **24** (1989) 2047.
15. B. D. CULLITY, "Elements of X-ray Diffraction", 2nd edn (Addison-Wesley, Reading, Massachusetts, 1978).
16. P. DREW and M. H. LEWIS, *J. Mater. Sci.* **9** (1974) 261.
17. M. SCHIMADA, A. TANAKA, T. YAMADA and M. KOIZUMI, "Densification and phase transformation of Si_3N_4 by high pressure sintering", in "Ceramic Powders" edited by P. Vincenzini (Elsevier, Amsterdam, 1983) pp. 871–9.
18. L. R. L. FALK, G. L. DUNLOP and R. POMPE, *Mater. Sci. Engng.* **71** (1985) 123.
19. F. F. LANGE, *Amer. Ceram. Bull.* **62** (1983) 1369.
20. A. G. EVANS and J. V. SHARP, "Transmission electron microscopy of silicon nitride", in "Electron Microscopy and structure of materials", edited by G. Thomas, R. M. Fulrath and R. M. Fisher (University of California Press, Berkley, 1972) pp. 1141–54.
21. R. W. K. HONEYCOMBE, "The plastic deformation of metals" (Arnold, London, 1968) Ch. 10.
22. J. W. MARTIN and R. D. DOHERTY, "Stability of microstructure in metallic systems", Cambridge solid state science series (Cambridge University Press, 1976) Ch. 3.
23. J. E. BAILEY and P. B. HIRSCH, *Proc. Roy. Soc.* **A267** (1962) 11.
24. A. COTTRELL, "An introduction to metallurgy", 2nd edn. (Arnold, London, 1975) Ch. 19.

Received 16 March
and accepted 4 September 1989